ENGINEERING Information Technology & Electronic Engineering
https://www.academax.com/EITEE; https://www.engineering.org.cn
https://ieeexplore.ieee.org/xpl/RecentIssue.jsp?punumber=11344065
E-mail: eng.itee@zju.edu.cn

Engineering Journals
Available on IEEE Xplore®

Research Article
https://doi.org/10.1631/ENG.ITEE.2025.0149

A dual-band filtering push–pull power amplifier with a large frequency ratio employing a hybrid-mode bandpass response balun

Jiyang CHU, Xiang WANG✉, Tianxiang CHEN, Jindong ZHANG, Jun HU, Huangyan LI, Boyu SIMA, Wen WU

School of Electronic and Optical Engineering, Nanjing University of Science and Technology, Nanjing 210094, China

Abstract: A dual-band filtering push–pull power amplifier (PA) with a large frequency ratio is presented in this paper. The proposed filtering power dividing/combining network is based on a hybrid-mode filtering balun using microstrip line (MSL) and substrate integrated waveguide (SIW). The MSL filtering balun operates in the S-band, with a frequency range of 2.6–2.86 GHz. Meanwhile, the SIW filtering balun is designed for Ku-band operation, covering a frequency range of 13–13.65 GHz. Under these conditions, the prototype is capable of attaining a frequency ratio as high as five times the original value. Due to the inherent differential characteristic of the hybrid-mode filtering balun with a large frequency ratio, the proposed push–pull PA not only realizes filtering functionality but also achieves second-harmonic suppression. To validate the designed concept, the proposed prototype has been designed, fabricated, and measured. Measurement results demonstrate that the proposed PA achieves a 7 dB small-signal gain while maintaining out-of-band spurious rejection during active testing. The developed dual-band filtering push–pull PA delivers excellent performance, with a peak output power of 36.8 dBm at low frequencies and 36 dBm at high frequencies. Moreover, by employing dual-band filtering baluns, the PA inherently suppresses even-order harmonics while simultaneously providing filtering characteristics in both operational bands, which effectively suppresses near-band spurious signals.

Key words: Large frequency ratio; Dual-band filtering balun; Harmonic suppression; Push–pull power amplifier

1 Introduction

With the rapid advancement of the 5th generation (5G) communication and radar technologies, the demand for high-power microwave components has grown substantially, spurring extensive research in this field. However, constrained by the limitations of semiconductor technology, the output power of individual devices remains inherently constrained. To address this challenge, push–pull power amplifiers (PAs) have attracted extensive research attention (Jobs et al., 2018; Chen WJ et al., 2020; Tiwari et al., 2020; Dong et al., 2022; Chen JX et al., 2024; Fahmi et al., 2025; Koh et al., 2025; Liu and Zhang, 2025; Zhou et al., 2025). These systems manipulate the superposition of electromagnetic waves to combine multiple low-power signals into a single high-power output.

For instance, a broadband power combiner based on a ridge waveguide was introduced by Dang et al. (2020), operating from 18 to 40 GHz and ultimately achieving a peak output power of 3.9 W by combining outputs from 16 gallium arsenide (GaAs) monolithic microwave integrated circuit (MMIC) PAs. Similarly, a push–pull PA presented by Feng WJ et al. (2019) uses two back-to-back filtering baluns to perform power combining while achieving a power-added efficiency (PAE) of 48.7% and effectively suppressing second-harmonic signals. As a device capable of providing differential signals, a balun is particularly suitable for push–pull power combining applications where harmonic suppression is required (Chiu et al., 2006; Stameroff et al., 2013; Geng et al., 2016; Wang et al., 2016; Feng LP and Zhu, 2017; Huang et al., 2019; Naeini et al., 2020; Shi et al., 2024; Steele and Psychogiou, 2024; Guo X et al., 2025).

Push–pull PAs have been designed and implemented across various transmission line technologies. Alternatively, hybrid-mode transmission lines have been widely adopted in multiple microwave devices owing to their high integration, compact size, and multifunctionality (Guo JP and Wu, 2018; Tang et al., 2019; Zhang et al., 2021; Ning et al., 2025). By using two microwave devices with distinct transmission line structures but similar functionalities, the hybrid-mode transmission line enables multiple functions while maintaining a compact form factor. For instance, the design presented by Tang et al. (2019) integrates two filters based on microstrip line (MSL) and waveguide technologies, separately, allowing operations in two distinct frequency bands without increasing the overall footprint and with the minimal mutual interference.

This paper presents a dual-band filtering push–pull PA with a large frequency ratio, designed using a hybrid configuration that

✉ Xiang WANG, wangxiang@njust.edu.cn
Xiang WANG, https://orcid.org/0000-0002-0320-7790
CLC number: TN722

Received: Nov. 20, 2025; Revision accepted: Jan. 13, 2026;
Crosschecked: Jan. 27, 2026

combines an MSL-based filtering balun and a substrate integrated waveguide (SIW)-based filtering balun. The low-frequency MSL filtering balun features a symmetric output topology, where a 180° phase difference between the output signals is achieved by adjusting the relative position of the input terminal, while filtering characteristics are realized through stepped impedance resonators (SIRs). In addition, the high-frequency SIW filtering balun generates phase-inverted output signals by exciting the vertical TM_{110} higher-order mode within the SIW cavity. These two filtering baluns are integrated and coupled via slots etched on the surface of the middle conductor between two dielectric substrates. Through the adoption of a back-to-back architecture to amplify and combine the differential signals generated by the filtering baluns, the proposed prototype achieves high output power with a large-frequency-ratio dual-passband filtering response and effective even-order harmonic suppression. These features are further validated by experimental results.

2 Design architecture

Fig. 1 illustrates the architectures of various push–pull PAs. Specifically, the conventional push–pull PA architecture is presented in Fig. 1a. A conventional push–pull PA comprises three stages: power division, power amplification, and power combining. First, the power divider splits the input signal into multiple paths of in-phase signals with equal amplitude, which are then amplified by PAs and finally combined in the power combining stage, thereby generating an output signal with significantly higher power than the achievable limit of a single amplifier. Fig. 1b depicts the architecture of a push–pull PA implemented with balun-based power dividers. Distinguished from the configuration in Fig. 1a, this configuration specifically employs baluns instead of standard power dividers for both power splitting and combining functions. Fig. 1c presents the architecture of a push–pull PA based on filtering baluns. Building upon the push–pull structure shown in Fig. 1b, this design replaces conventional baluns with filtering baluns, thereby incorporating filtering characteristics into the push–pull PA. Consequently, Fig. 1d demonstrates the design of a dual-band filtering push–pull PA based on hybrid-mode transmission lines. Evolving from the architecture in Fig. 1c, this design incorporates dual-band filtering baluns for power division and power combining, enabling dual-band operation while maintaining the functionalities of the original filtering push–pull network within both operational bands.

Owing to its inherent differential-output architecture, a balun intrinsically delivers odd harmonics (including the fundamental tone) as differential-mode signals, while even harmonics manifest as common-mode signals. Once the differential signals output from the balun are amplified, the two PAs exhibit strong nonlinearity, delivering outputs with identical amplitude, opposite phase, and high saturated power. This nonlinear behavior can be mathematically represented as follows:

$$i_1=a_1v+a_2v^2+a_3v^3+\ldots, \tag{1}$$

$$i_2=a_1v\mathrm{e}^{-\mathrm{j}\pi}+a_2(v\mathrm{e}^{-\mathrm{j}\pi})^2+a_3(v\mathrm{e}^{-\mathrm{j}\pi})^3+\ldots, \tag{2}$$

where v denotes the input voltage, i_1 and i_2 represent the output currents, and the parameter a_i governs the transfer function of the PAs. The two signals amplified by the PAs are combined by a balun, which merges the two out-of-phase input signals into one combined signal. Synthesizing Eqs. (1) and (2) yields Eq. (3), revealing that the composite output current reinforces the fundamental component while suppressing even-order harmonics, a key benefit of the push–pull architecture. The total current synthesized from the two paths can be expressed as

$$i=i_1+i_2^{-\mathrm{j}\pi}=2a_1v+2a_3v^3+\ldots. \tag{3}$$

The proposed dual-band filtering push–pull PA, using dual-band filtering baluns and operating with a large frequency ratio, achieves a significant enhancement in output power compared to conventional architectures. Furthermore, it effectively suppresses even-order

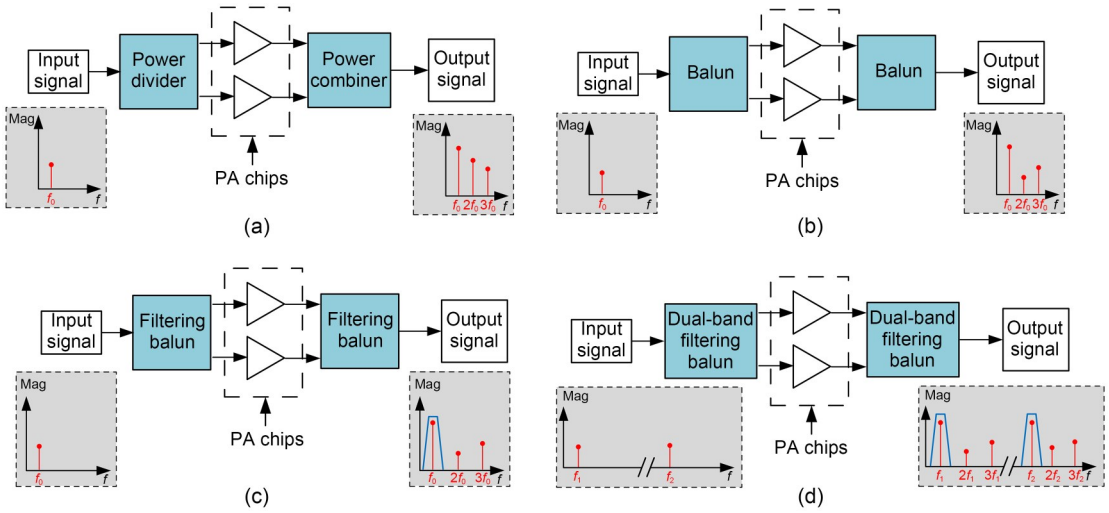

Fig. 1 Architectures of various push–pull PAs: (a) conventional push–pull PAs; (b) push–pull PAs employing baluns; (c) filtering push–pull PAs; (d) dual-band filtering push–pull PAs. The horizontal axis *f* represents the frequency (in GHz), and the vertical axis "Mag" represents the magnitude of the input signal (in dBm). f_0 represents the operating frequency of a conventional push–pull PA, while f_1 and f_2 represent the two operating frequencies of the dual-band push–pull filtering PA

harmonics and their associated spurious components. Moreover, the adoption of filtering baluns for power combining enables effective rejection of near-band spurious responses in both operating bands. This approach achieves dual-band filtering characteristics while avoiding the size penalty associated with cascaded external filters.

3 Dual-band filtering balun and filtering push–pull PA with a large frequency ratio

3.1 Large-frequency-ratio dual-band filtering balun

Fig. 2a illustrates a three-dimensional (3D) view of the proposed dual-band filtering balun with a large frequency ratio. The designed prototype comprises two types of filtering baluns: an MSL filtering balun and an SIW filtering balun.

The MSL filtering balun is designed based on a Marchand balun architecture (Lin et al., 2015; Geng et al., 2016). It consists of a section of impedance-transforming line, a stepped-impedance low-pass filter (LPF), two $\lambda/2$ uniform-impedance resonators (UIRs), and two $\lambda/2$ SIRs, where λ is the wavelength at the center frequency of the proposed MSL filtering balun. The low-frequency signal is introduced into the MSL filtering balun from the unbalanced port 1 and is guided through the impedance-transforming line. Subsequently, the input signal is fed into the LPF, which is designed to isolate the two operating bands, thereby preventing the low-frequency signal from interfering with the high-frequency filtering balun. The configuration employs two UIRs and two SIRs arranged in a combined configuration. Under differential-mode excitation, the odd-mode half-circuit is formed by four quarter-wavelength resonators. With mixed differential-mode coupling between the UIR and SIR, the coupling between the two SIRs is predominantly electric.

The design methodology of the MSL filtering balun is outlined as follows:

1. Topology selection and initial sizing. The balun is based on a modified Marchand topology, chosen for its inherent wideband differential performance. The $\lambda/2$ UIRs and SIRs are initially dimensioned using standard transmission-line equations at the center frequency. The SIRs are employed primarily to introduce an additional transmission zero for improved out-of-band rejection and to provide an extra degree of freedom for bandwidth control.

2. Bandwidth matching. The target bandwidth is achieved by controlling the coupling coefficients between the resonators and the feed lines. The couplings are tuned by adjusting the gaps between adjacent resonators and the length/width of the coupling sections.

3. Phase and amplitude imbalance optimization. As for the phase characteristic, the fundamental 180° phase difference is structurally enforced by the laterally offset input feed line, and fine-tuning of the phase balance is achieved by slightly adjusting the electrical lengths of the two output paths, specifically by optimizing the meandered output lines. As for the amplitude characteristic, amplitude balance between the two output ports is optimized by ensuring symmetrical geometry and by carefully adjusting the impedance transformer at the input to provide equal excitation to both signal paths.

Figs. 2b and 2c present the detailed layouts and dimensional parameters of the MSL filtering balun and SIW filtering balun, respectively. A Rogers 4003 substrate (the relative permittivity of the substrate ε_r=3.55, the thickness of the substrate h=0.813 mm, and the dielectric loss tangent of the substrate tanδ_D=0.0027) is used for this design. The corresponding parameters are summarized in Fig. 2.

Fig. 2c depicts the top view of the lower substrate. The high-frequency signal entering the same port 1 is directly coupled into the SIW filtering balun through the rectangular slot etched at the bottom of the upper substrate. It should be mentioned that the low-pass filter cascaded with the MSL filtering balun prevents this upper branch from interfering with the high-frequency response.

As two orthogonal degenerate modes of the circular SIW resonator, the vertical TM_{110} mode and the horizontal TM_{110} mode exhibit electric field distributions oriented 90° apart (Li P et al., 2015; Li HY et al., 2019). The field distribution of the vertical TM_{110} mode in the circular cavity demonstrates odd symmetry, characterized by equal magnitude but opposite phase on either side of the

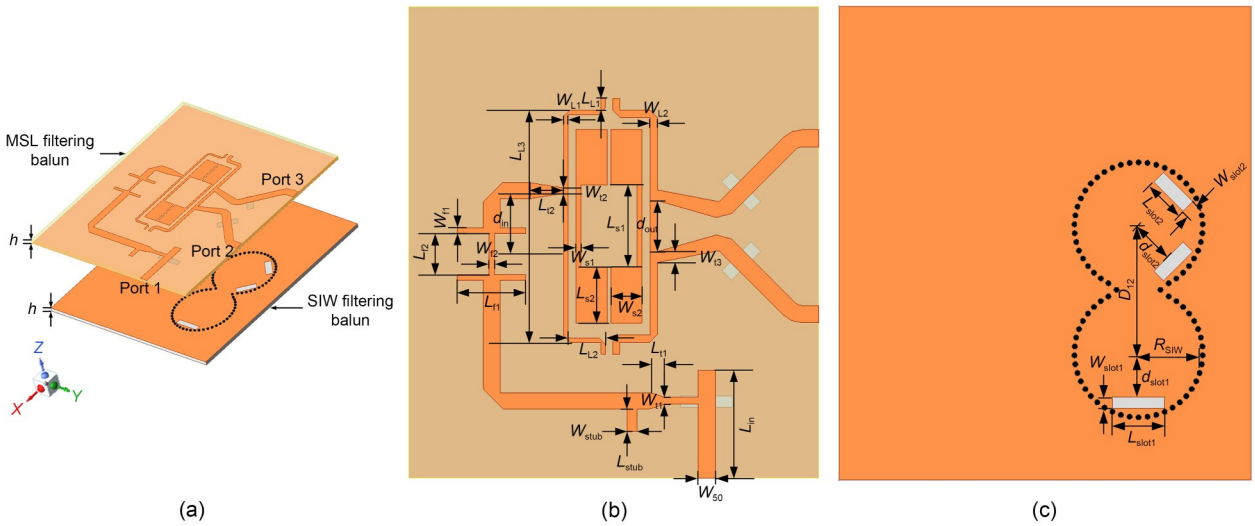

Fig. 2 Structure of the large-frequency-ratio dual-band filtering balun: (a) 3D view of the proposed bandpass filtering balun; (b) top view of the upper substrate; (c) top view of the lower substrate. Parameters in (b) and (c) are W_{50}=1.88, L_{in}=11.8, L_{t1}=1.6, W_{t1}=0.8, L_{stub}=2.5, W_{stub}=1.1, L_{f1}=7.5, W_{f1}=0.6, L_{f2}=4.5, W_{f2}=0.6, d_{in}=3.6, L_{t2}=3.8, W_{t2}=0.58, L_{L1}=1.3, L_{L2}=4.1, L_{L3}=25.4, W_{L1}=0.45, W_{L2}=0.8, L_{s1}=9, W_{s1}=0.55, L_{s2}=6.1, W_{s2}=3.4, d_{out}=5.6, W_{t3}=1.18, R_{SIW}=7, D_{12}=13.8, d_{slot1}=4.8, W_{slot1}=1.2, L_{slot1}=5.7, d_{slot2}=4.6, W_{slot2}=1.5, L_{slot2}=4.5 (unit: mm). h is the thickness of the substrate

cavity center. In contrast, the horizontal TM_{110} mode exhibits even symmetry, with the field being identical in both magnitude and phase across the two symmetric halves. Consequently, the proposed second-order SIW filtering balun is designed based on the vertical TM_{110} mode of the circular SIW cavity.

The design methodology of the SIW filtering balun is outlined as follows:

1. Mode selection and cavity design. The balun operation is based on exciting the vertical TM_{110} mode in a circular SIW cavity. The dimensions of the cavity are first calculated to resonate at the desired center frequency for this mode using Eq. (4) for a circular cavity, with effective permittivity accounting for the SIW substrate.

$$f_{mnp}^{\mathrm{TM}}=\frac{c}{2\pi\sqrt{\varepsilon_{\mathrm{r}}}}\sqrt{\left(\frac{\chi_{mn}}{a}\right)^{2}+\left(\frac{p\pi}{h}\right)^{2}}, \tag{4}$$

where f_{mnp}^{TM} represents the resonant frequency of the TM mode, c denotes the speed of light in a vacuum, a is the effective radius of the SIW cavity, m, n, and p are the mode indices, and χ_{mn} denotes the n^{th} root of the m^{th}-order Bessel function $J_m(x)=0$, corresponding to the boundary conditions for the TM mode.

2. Bandwidth matching. A second-order bandpass response is implemented using two coupled cavities. The bandwidth is determined by the inter-cavity coupling, controlled by the coupling aperture between the cavities, and the input/output coupling, controlled by the dimensions of the coupling aperture.

3. Phase and amplitude imbalance optimization. The 180° phase difference is an inherent property of the selected vertical TM_{110} mode, which exhibits odd symmetry. The phase balance across the band is ensured by symmetrically positioning the two output coupling slots on opposite sides of the cavity center. The exact slot positions are fine-tuned to compensate for parasitic phase shifts introduced by the microstrip (MS) feed lines. The amplitude balance is achieved by the geometrical symmetry of the output slots. Their identical dimensions and symmetrical placement relative to the field maximum of the TM_{110} mode guarantee equal coupling to the two output ports.

Fig. 3 demonstrates the simulated electric-field distribution within the SIW cavity at 13.5 GHz. The plot confirms the excitation of the vertical TM_{110} mode, characterized by two anti-phase field distributions coexisting within the cavity. Two output coupling slots are positioned to efficiently extract these differential signals into the output MSLs, thereby realizing balun function. The signal is coupled from port 1 of the MS feed line through an aperture into the first circular SIW cavity, and the vertical TM_{110} mode is then excited within both cavities. When the signals are coupled to ports 2 and 3 of the MSL filtering balun, they exhibit equal amplitude and opposite phase. The corresponding geometrical parameters are provided in Fig. 2.

Following the individual design and optimization of the MSL and SIW filtering baluns, the co-design and integration considerations are considered as follows:

First, the LPF placed before the MSL balun is crucial for band isolation. Its cutoff frequency is set between the operating bands of the MSL and SIW filtering baluns, preventing the low-frequency signal from interfering with the SIW cavity's operation. Second, the final optimization of the entire hybrid structure is performed in a combined EM simulation, allowing for fine-tuning of all parameters to account for any unintended cross-coupling between the MSL and SIW sections, ensuring that the bandwidth matching targets and phase/amplitude balance are satisfied simultaneously for both bands. The design flowchart of the proposed dual-band filtering balun is shown in Fig. 4.

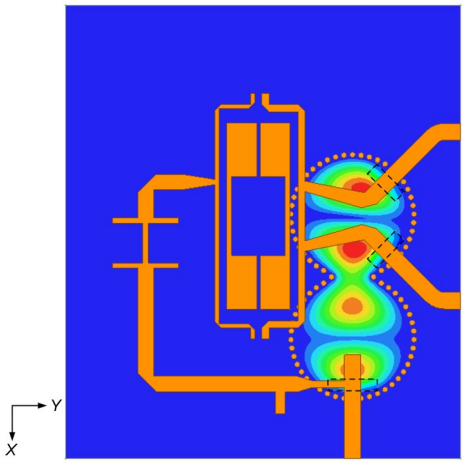

Fig. 3 Simulated electric-field distribution within the SIW cavity at 13.5 GHz

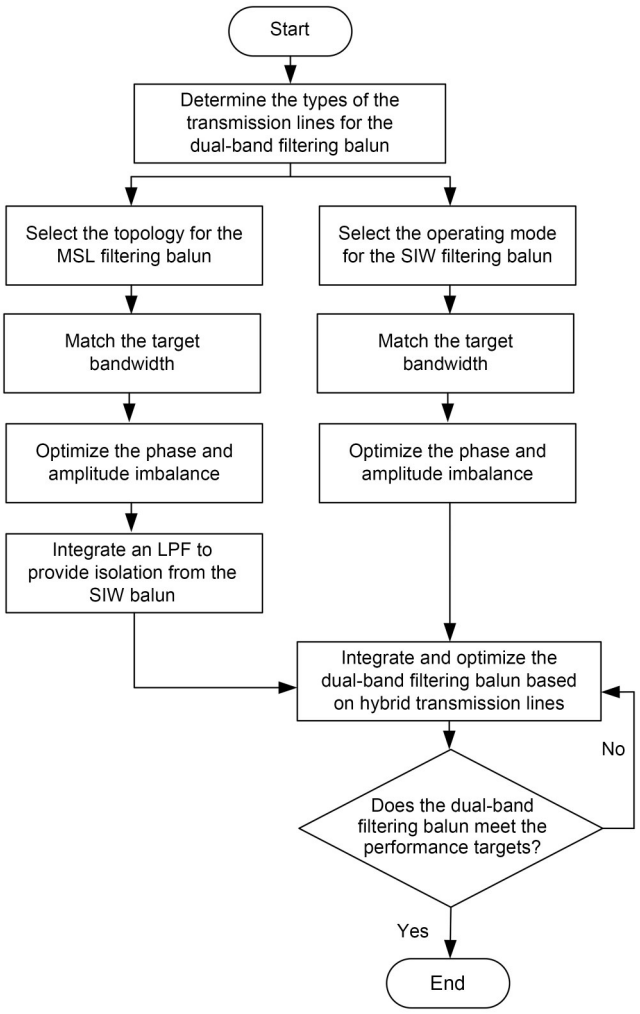

Fig. 4 Design flowchart of the proposed dual-band filtering balun

The final dual-band filtering balun achieves a fivefold frequency ratio. In this design, the attainable frequency ratio is constrained by both physical layout considerations and substrate performance limitations. First, physical layout dictates that the operating frequency cannot be too high or too low. If the frequency is too low, the physical size of the SIW cavity becomes significantly larger than that of the MSL structure, leading to layout conflicts and potential unwanted coupling between resonators. Moreover, the coupling aperture at the SIW input is positioned far from the MSL input port. To enable port reuse at the input of the dual-band filtering balun, a long, curving MS feed line is needed to connect them, thereby introducing excessive loss into the low-frequency filtering balun. Conversely, an excessively large frequency ratio leads to a tiny SIW cavity. The proper operation of the SIW balun depends on exciting the TM_{110} mode, whose field symmetry dictates that the output coupling slots must be placed symmetrically to generate differential signals. For port reuse, these slots must cover the MS output feed lines. A small radius R_{SIW} makes it difficult to satisfy both the mode symmetry requirement and the port reuse constraint simultaneously without significant performance degradation.

Second, for the SIW balun, the substrate thickness must satisfy $h<\lambda_g/4$ (λ_g represents the guided wavelength) to minimize radiation loss and suppress higher-order vertical modes. For the MSL balun, conversely, its power handling capability and quality factor generally benefit from a thicker substrate. Therefore, selecting a substrate involves a trade-off that defines the range of the ratio between the pair of low and high operating frequencies.

Our design, with a fivefold frequency ratio, successfully balances these opposing constraints, providing ample space for the MSL structure to wrap around the SIW cavity without a significant loss penalty.

As a design trade-off, the relatively large footprint of the proposed MSL–SIW hybrid structure can be considered as a consequence of integrating two distinct transmission-line technologies to achieve a large-frequency-ratio dual-band filtering functionality within a single module. Because the MSL filtering balun operates at relatively low frequencies, primarily in the S-band, and employs $\lambda/2$ UIRs and SIRs to achieve its filtering response, it inherently results in a larger footprint. In addition, to enable coupling with the MSL filtering balun at both the input and output ports, the size of the SIW filtering balun cannot be designed excessively compact.

3.2 Large-frequency-ratio dual-band filtering push–pull PA

The proposed dual-band filtering balun with a large frequency ratio is employed to implement a back-to-back active dual-band filtering push–pull PA architecture.

Fig. 5 demonstrates the physical configuration of the proposed active dual-band hybrid filtering push–pull PA with a large frequency ratio. A low-pass filter is incorporated before the MSL filtering balun to prevent any adverse effect on the performance of the SIW filtering balun. The input signal is first processed by the LPF and then fed into the MSL filtering balun, which outputs two differential signals of equal amplitude. These two signals are subsequently amplified by separate wideband PA chips and finally combined, exploiting an identical filtering balun configuration. For the high-frequency path, the input signal is directly coupled into the SIW cavity. After processing, the output signal is coupled into the MS output feed lines. This configuration enables the high-frequency and low-frequency sections to share common input and output ports, significantly enhancing the overall integration level and practical applicability of the design.

The filtering push–pull PA operates by dividing an input low-power signal, separately amplifying the resulting signals and synthesizing them to achieve an output power greater than that available from a single PA chip. As outlined in Section 2, amplifying the differential-mode signals before synthesis provides the dual advantage of fundamental wave amplification and second-harmonic suppression. Leveraging this principle, the proposed filtering dual-band PA employs a back-to-back structure incorporating the designed dual-band hybrid-mode filtering baluns. This configuration not only preserves the inherent dual-band filtering characteristics of the baluns but also simultaneously provides both signal amplification and second-harmonic suppression.

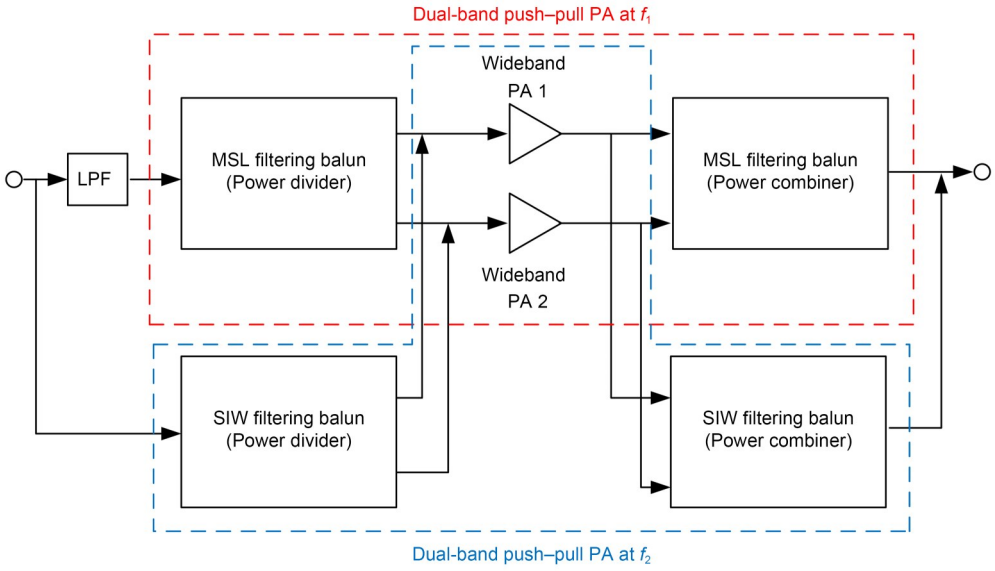

Fig. 5 Architecture of the proposed hybrid-mode dual-band filtering push–pull PA with a large frequency ratio

4 Implementation and measurement

For a practical demonstration, the dual-band filtering push–pull PA with a large frequency ratio designed in the previous section has been manufactured and characterized. The proposed filtering balun at low frequency, employing MS resonators, is designed on the top substrate. Meanwhile, the filtering balun at high frequency, exploiting SIW resonators, is manufactured on the bottom substrate. The determined parameters are listed in Fig. 2.

The assembly layouts of the large-frequency-ratio dual-band filtering balun are displayed in Fig. 6. The MSL and SIW filtering baluns are fabricated on two separate dielectric substrates with identical material. To facilitate the experiment and minimize the performance impact on the dual-band filtering balun, the low- and high-frequency baluns are arranged in a stacked configuration, as depicted in Fig. 2a, and secured with nylon screws.

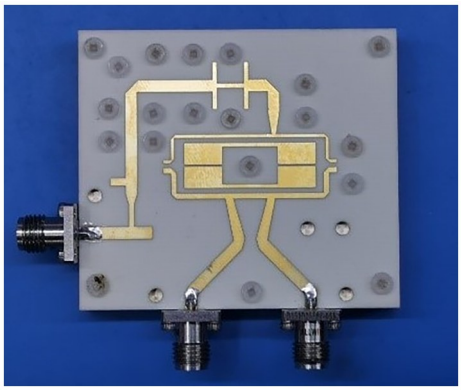

Fig. 6 Assembly layouts of the proposed large-frequency-ratio dual-band filtering balun

Fig. 7 illustrates the simulation and measurement results of the dual-band filtering balun. Figs. 7a and 7b present the simulated and measured *S*-parameters of the low-frequency and high-frequency filtering baluns, respectively. For the low-frequency filtering balun, the measurement results indicate a return loss better than 19 dB over the 2.60–2.86 GHz band and an insertion loss of 1.3 dB after excluding the contributions from SubMiniature version A (SMA) connectors and microwave cables. Meanwhile, the measurement of the high-frequency SIW filtering balun indicates a return loss better than 13.5 dB and an insertion loss of 2.3 dB in the 13–13.65 GHz range, after de-embedding the effects of SMA connectors and microwave cables. Furthermore, the corresponding simulated and measured phase difference of the low-frequency and high-frequency filtering baluns are shown in Figs. 7c and 7d, respectively. Both simulation and measurement indicate that the phase difference between the two output ports is maintained at 180° with a deviation of ±5° throughout their operational bands, demonstrating excellent phase balance.

Fig. 8 shows the assembly layouts and experimental configuration for the proposed devices. Specifically, Fig. 8a presents the detailed assembly layouts of the large-frequency-ratio dual-band filtering push–pull PA. Two of the developed dual-band filtering baluns function as the input power divider and output power combiner, separately. Between them, two broadband gallium nitride (GaN) MMIC PA modules are integrated to amplify the signals, thereby enabling experimental validation of the complete active push–pull PA. To achieve a higher saturated output power, an identical PA module is placed before the input filtering balun to drive the entire push–pull PA.

To characterize the proposed concept, a test setup based on the large-frequency-ratio dual-band filtering push–pull PA is implemented. The schematic illustration and photograph of the test environment

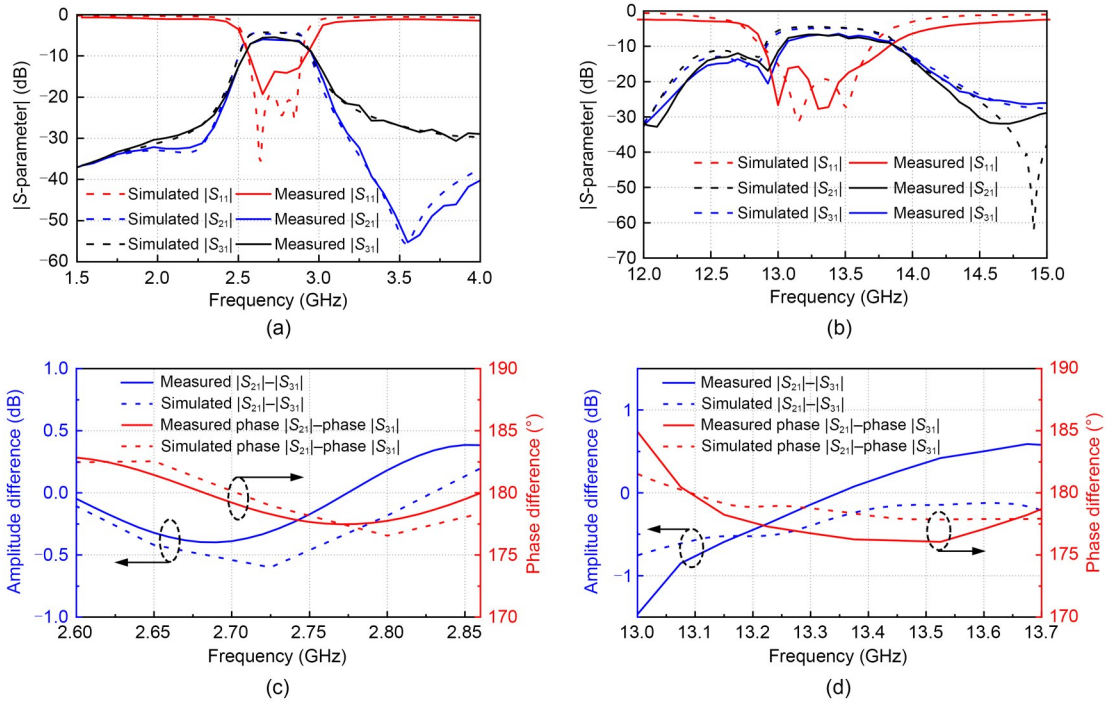

Fig. 7 Simulation and measurement results of the proposed dual-band hybrid filtering balun: (a) low-frequency response; (b) high-frequency response; (c) phase difference in the low-frequency band; (d) phase difference in the high-frequency band. S_{11} represents the return loss at port 1, while S_{21} and S_{31} represent the insertion losses at ports 2 and 3, respectively

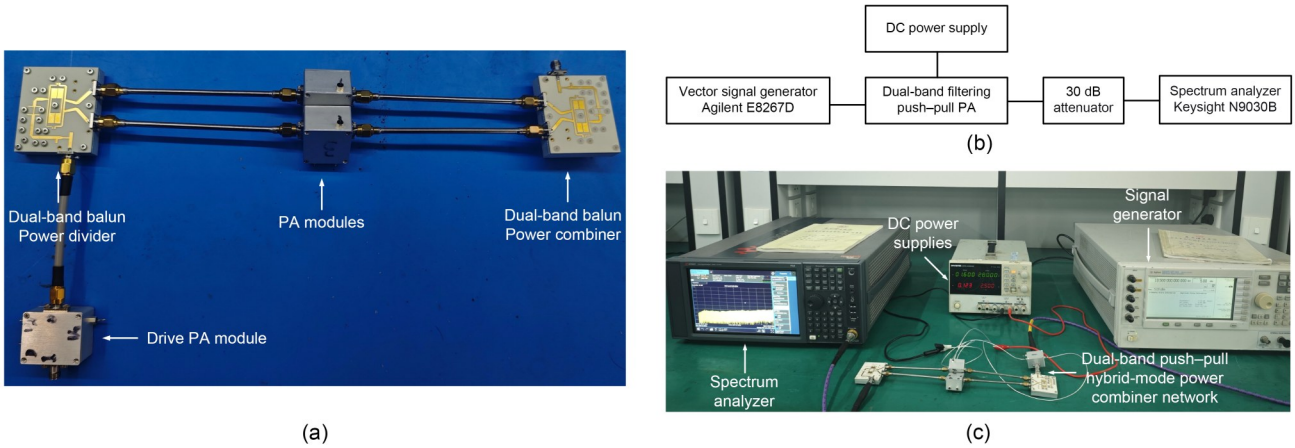

Fig. 8 Assembly layouts and experimental configuration for the proposed devices: (a) assembly diagram of the dual-band filtering push–pull PA; (b) test schematic illustration of the dual-band filtering push–pull PA; (c) experimental environment of the proposed dual-band filtering push–pull PA

are depicted in Fig. 8b and Fig. 8c, respectively. The input signal from an Agilent E8267D signal generator is first amplified by the external PA module to compensate for its limited output power, and is further amplified by the specifically designed dual-band filtering push−pull PA. All PAs used in the design are biased by a direct current (DC) power supply, and the final output is measured by a Keysight N9030B spectrum analyzer via a 30 dB attenuator. The PA chips are biased at a gate voltage of −1.8 V and a drain voltage of +28 V, and operate with a quiescent current of 440 mA.

The measured small-signal gain and dual-band spectral responses are presented in Figs. 9 and 10, respectively. As shown in Fig. 9, the implemented filtering push–pull PA maintains a consistent 7 dB small-signal gain across both operational bands, with bandwidths aligning closely with the passive measurement results shown in Fig. 7a. Due to the inherent gain flatness variations in the employed MMIC PA chips, the designed PA exhibits some in-band gain fluctuations. Furthermore, the system maintains excellent filtering performance during active testing, demonstrating effective suppression of out-of-band spurious components.

The spectral response of the dual-band filtering push−pull PA operating in its low-frequency band under a 2.75 GHz input signal is presented in Fig. 10a. The low-frequency saturated output power of the PA is 36.8 dBm, while the second harmonic at 5.50 GHz is effectively suppressed, with its output power measured at −54.7 dBm. Furthermore, under a 13.50 GHz input signal, Fig. 10b displays the

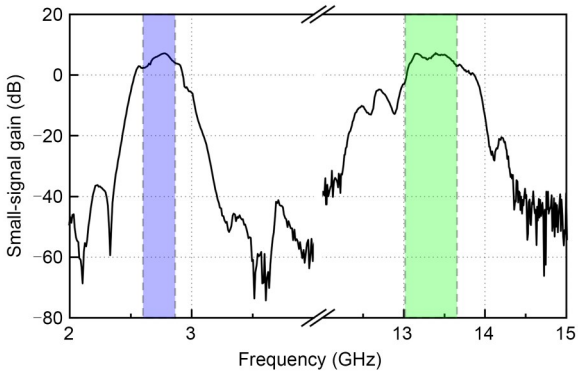

Fig. 9 Measured small-signal gain of the proposed dual-band filtering push–pull PA

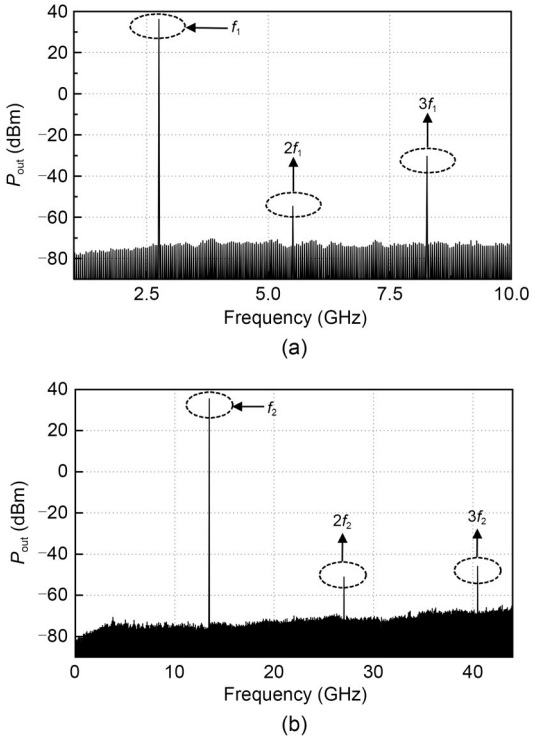

Fig. 10 Measurement results of the proposed dual-band filtering push–pull PA: (a) low-frequency measured result; (b) high-frequency measured result. P_{out}: the output power of the PAs

spectral response of the dual-band filtering push–pull PA operating in its high-frequency band. A saturated output power of 36 dBm is observed in the high-frequency band. Additionally, the second harmonic at 27 GHz is strongly suppressed, with its output power measured at −53 dBm. The slight difference in the peak output power between the bands is attributed to the frequency-dependent gain variation of the broadband PA chips.

Table 1 summarizes and compares the performance of various state-of-the-art designs and our design. Using the radial waveguide power combining technique, Koh et al. (2025) achieved a 0.5 W output in the W-band, whereas our work achieves a peak output power superior by 10 dB. Although the broadband 24-way radial power-combining network in Liu and Zhang (2025) demonstrates

Table 1 Performance comparison between this work and prior studies

Method	Type	Number of operating bands	Frequency (GHz)	R_f	P_{out} (dBm)	Filtering function	N-way	Harmonic suppression	Footprint (λ_g^3)
Koh et al. (2025)	Waveguide	1	93–101	N/A	26.72	No	8	No	24×26×6.5
Liu and Zhang (2025)	Waveguide	1	26–42	N/A	54.7	No	24	No	11×11×4.3
Dang et al. (2020)	RIWG	1	18–40	N/A	35.9	No	16	No	3.4×2.6×2.2
Feng WJ et al. (2019)	SIW	1	5.4–5.6	N/A	38.5	Yes	2	Yes	5.6×4.7×0.03
Li SB et al. (2023)	MSL	2	2.1/3.5	1.7	41.0/39.5	Yes	1	Yes	–
Chen H et al. (2022)	MSL	2	2.14/2.60	1.2	43.25/43.3	Yes	2	Yes	–
Kim and Oh (2024)	HCDMN	2	2.20–2.25/3.30–3.45	1.5	40.3/41.9	Yes	1	Yes	1×0.73×0.01
Our work	MSL–SIW	2	2.60–2.86/13–13.65	5	36.8/36	Yes	2	Yes	0.77×0.88×0.03

R_f represents the frequency ratio of the dual-band PAs. Footprint: the physical dimensions of the mentioned designs. N-way: the number of channels in the multi-way push–pull PAs. N/A represents not applicable. "–" represents not available

improved isolation and the highest output power to date, it does not incorporate any filtering capabilities. An ultra-wideband ridge waveguide (RIWG) power-combining method is presented in Dang et al. (2020). It features a bandwidth covering K to Ka bands, while its harmonic suppression capability is limited. Feng WJ et al. (2019) presented an SIW-based filtering push−pull PA that provides harmonic suppression. In contrast, our work extends this concept to dual-band operation through the use of hybrid transmission lines, enabling filtering and harmonic suppression in two frequency bands. Li SB et al. (2023) presented a diplexer-like dual-band filtering PA, which operates at 2.1/3.5 GHz, delivering output powers of 41.0 and 39.5 dBm at two frequencies, achieving second-harmonic suppression. Multi-functional circuits have been employed in the design of dual-band filtering PAs (Chen H et al., 2022). By allowing the power combiner and the filtering circuits to share a common resonator, the overall circuit size can be reduced. A dual-band PA based on a harmonic-controlled dual-band matching network (HCDMN) has been proposed in Kim and Oh (2024). The HCDMN comprises $\lambda/4$ open stubs for suppressing second-harmonic signals, and saturated P_{out} values of 40.3 and 41.9 dBm at 2.30 and 3.35 GHz, respectively. However, it is generally challenging for dual-band PAs to achieve a large frequency ratio by implementing a single-circuit configuration based on the same type of transmission line.

Attributing to the MSL−SIW hybrid architecture, the proposed dual-band filtering PA achieves optimized spatial utilization, insertion loss, and power handling capacity by combining the strengths of both technologies, compared to using a single transmission line. The SIW section of the hybrid architecture enables flexible mode selection, which provides differential output for balun operation through mode control. With its high Q-factor and excellent electromagnetic shielding properties, the hybrid architecture provides steeper out-of-band suppression and superior passband selectivity, which offers an effective design pathway for high-performance, compact dual-band filtering power amplifiers.

5 Conclusions

In this paper, a dual-band filtering push−pull PA with a large frequency ratio using hybrid-mode filtering baluns is designed, fabricated, and measured. First, a dual-band filtering balun with a large frequency ratio is designed based on an MSL–SIW hybrid structure. Subsequently, a dual-band filtering push−pull PA is developed using a back-to-back configuration, which uses the proposed filtering baluns and GaN MMIC PA modules. Based on the passive measurement results, the active small-signal power gain and saturated output spectra are characterized. Simulation and measurement results show satisfactory agreement. This work can provide effective guidance and a method for application scenarios with a large frequency ratio, such as 5G/6G base stations or user equipment.

Acknowledgments

This work was supported by the National Natural Science Foundation of China (No. 62201262) and the Fundamental Research Funds for the Central Universities (No. 30924010912).

Author contributions

Jiyang CHU designed the research, processed the data, and drafted the paper. Xiang WANG processed the data and helped organize the paper. Tianxiang CHEN processed the data. Jindong ZHANG conducted the theoretical analysis and supervised the work. Jun HU conducted the theoretical analysis. Huangyan LI conducted the theoretical analysis and supervised the work. Boyu SIMA conducted the theoretical analysis and developed the methodology. Wen WU provided resources, supervised the work, and contributed to validation. All the authors revised and finalized the paper.

Conflict of interest

All the authors declare that they have no conflict of interest.

Data availability

The data that support the findings of this study are available from the corresponding author upon reasonable request.

Declaration on the use of generative AI tools

During the preparation of this work, the authors used ChatGPT to improve language. After using this tool, the authors reviewed and edited the content as needed and take full responsibility for the content of the published article.

References

Chen H, Xu JX, Chen WH, et al., 2022. High-efficiency dual-band filtering Doherty power amplifier based on multi-function circuit. *IEEE Trans Microw Theory Tech*, 70(5):2697-2709. https://doi.org/10.1109/TMTT.2022.3154756

Chen JX, Shi X, Xue Y, et al., 2024. A compact and low loss filtering balun based on asymmetrical ridge waveguide resonator. *IEEE Microw Wirel Technol Lett*, 34(12): 1327-1330. https://doi.org/10.1109/LMWT.2024.3474034

Chen WJ, Wu YL, Wang WM, 2020. Wideband bandpass filtering balun with perfect in-band matching and isolation. *IEEE Trans Circ Syst II Express Briefs*, 67(10): 1884-1888. https://doi.org/10.1109/TCSII.2019.2955145

Chiu L, Yum TY, Xue Q, et al., 2006. A wideband compact parallel-strip 180° Wilkinson power divider for push–pull circuitries. *IEEE Microw Wirel Compon Lett*, 16(1):

49-51. https://doi.org/10.1109/LMWC.2005.859972

Dang Z, Zhu HF, Huang J, et al., 2020. An ultra-wideband power combining in ridge waveguide for millimeter wave. *IEEE Trans Microw Theory Tech*, 68(4):1376-1389. https://doi.org/10.1109/TMTT.2019.2963861

Dong GY, Yang XL, Fang YN, et al., 2022. Filtering push–pull power amplifier based on multifunctional impedance matching network. *IEEE Microw Wirel Compon Lett*, 32(5):422-425. https://doi.org/10.1109/LMWC.2021.3136718

Fahmi MM, MacDonald ME, Fathy AE, et al., 2025. 50-way W-band all waveguide radial combiner design. *IEEE Microw Wirel Technol Lett*, 35(6):792-795. https://doi.org/10.1109/LMWT.2025.3554515

Feng LP, Zhu L, 2017. Wideband filtering balun on a novel hybrid multimode resonator with the functionality of vertical transition. *IEEE Trans Compon Packag Manuf Technol*, 7(8):1324-1330. https://doi.org/10.1109/TCPMT.2017.2658669

Feng WJ, Shi YR, Zhou XY, et al., 2019. A bandpass push–pull high power amplifier based on SIW filtering balun power divider. *IEEE Trans Plasm Sci*, 47(9):4281-4286. https://doi.org/10.1109/TPS.2019.2932083

Geng YF, Wang WW, Chen XW, et al., 2016. The study and design of a miniaturized microstrip balun with a wider bandwidth. *IEEE Antenn Wirel Propag Lett*, 15:1727-1730. https://doi.org/10.1109/LAWP.2016.2530142

Guo JP, Wu K, 2018. Half-mode composite waveguide. *IEEE Trans Microw Theory Tech*, 66(6):2920-2927. https://doi.org/10.1109/TMTT.2018.2825395

Guo X, Tao Y, Wu W, 2025. High-frequency balun with compact size and low loss on self-packaged air-filled suspended line. *IEEE Trans Compon Packag Manuf Technol*, 15(2):356-366. https://doi.org/10.1109/TCPMT.2024.3501401

Huang F, Wang JP, Aliqab K, et al., 2019. Analysis and design of a new self-packaged wideband balun bandpass filter with the functionality of impedance transformation. *IEEE Trans Microw Theory Tech*, 67(6):2322-2330. https://doi.org/10.1109/TMTT.2019.2905563

Jobs M, Dancila D, Eriksson J, et al., 2018. An 8-1 single-stage 10-kW planar Gysel power combiner at 352 MHz. *IEEE Trans Compon Packag Manuf Technol*, 8(5):851-857. https://doi.org/10.1109/TCPMT.2018.2811710

Kim B, Oh J, 2024. Dual-band continuous class-F^{-1} power amplifier with second-harmonic suppression for harmonic radar systems. *IEEE Access*, 12:62358-62364. https://doi.org/10.1109/ACCESS.2024.3395518

Koh Y, Yi C, Kim M, 2025. W-band 0.5-W waveguide module utilizing spatial power combining of linear amplifier array. *IEEE Microw Wirel Technol Lett*, 35(9):1396-1399. https://doi.org/10.1109/LMWT.2025.3570639

Li HY, Xu JX, Zhang XY, 2019. Substrate integrated waveguide filtering rat-race coupler based on orthogonal degenerate modes. *IEEE Trans Microw Theory Tech*, 67(1):140-150. https://doi.org/10.1109/TMTT.2018.2874252

Li P, Chu H, Chen RS, 2015. SIW magic-T with bandpass response. *Electron Lett*, 51(14):1078-1080. https://doi.org/10.1049/el.2015.0640

Li SB, Wu YL, Xu ZY, et al., 2023. A diplexer-like dual-band filtering power amplifier with selectable frequency output. *IEEE Microw Wirel Technol Lett*, 33(12):1626-1629. https://doi.org/10.1109/LMWT.2023.3311193

Lin SC, Hsieh CW, Wang CC, et al., 2015. Bow-tie antenna fed by microstrip balun filter with designable bandwidth and extended stopband. European Microwave Conf, p.1053-1056. https://doi.org/10.1109/EuMC.2015.7345948

Liu HX, Zhang YH, 2025. A Ka-band broadband radial power combiner with high isolation among all input ports. *IEEE Trans Microw Theory Tech*, 73(10):8288-8298. https://doi.org/10.1109/TMTT.2025.3576125

Naeini MR, Mirmozafari M, van der Weide D, 2020. Monolithic 3-D printing of an integrated Marchand balun with a dipole antenna. *IEEE Trans Compon Packag Manuf Technol*, 10(4):654-658. https://doi.org/10.1109/TCPMT.2020.2966535

Ning K, Zhu YR, Liu XY, et al., 2025. Mode composite ridged substrate integrated coaxial line for multichannel operation. *IEEE Trans Microw Theory Tech*, 73(8):5203-5214. https://doi.org/10.1109/TMTT.2025.3531873

Shi X, Xue Y, Yang YJ, et al., 2024. A wideband DRWG balun with low loss and compact size. *IEEE Microw Wirel Technol Lett*, 34(4):379-382. https://doi.org/10.1109/LMWT.2024.3364667

Stameroff AN, Ta HH, Pham AV, et al., 2013. Wide-bandwidth power-combining and inverse class-F GaN power amplifier at X-band. *IEEE Trans Microw Theory Tech*, 61(3):1291-1300. https://doi.org/10.1109/TMTT.2013.2244611

Steele J, Psychogiou D, 2024. Self-packaged inkjet-printed vertically integrated RF co-designed bandpass filtering baluns. *IEEE Trans Compon Packag Manuf Technol*, 14(11):2124-2127. https://doi.org/10.1109/TCPMT.2024.3469868

Tang WS, Su ZL, Zheng SY, 2019. Dual-band bandpass filter with large frequency ratio and independently tunable center frequencies. IEEE MTT-S Int Wireless Symp, p.1-3. https://doi.org/10.1109/IEEE-IWS.2019.8804022

Tiwari RK, Jain S, Prasad G, 2020. Complementary compound push pull power amplifier for wide frequency band applications using CMOS nanotechnology. Int Conf on Electrical and Electronics Engineering, p.402-405. https://doi.org/10.1109/ICE348803.2020.9122903

Wang JP, Huang F, Zhu L, et al., 2016. Study of a new planar-type balun topology for application in the design of balun bandpass filters. *IEEE Trans Microw Theory Tech*, 64(9):2824-2832. https://doi.org/10.1109/TMTT.2016.2594257

Zhang XF, Cao SH, Chen JX, 2021. Novel millimeter-wave bandwidth-controllable filtering antenna based on composite ESPPs-SIW structure. *IEEE Trans Antenn Propag*, 69(11):7924-7929. https://doi.org/10.1109/TAP.2021.3088538

Zhou GQ, Xu J, Su JH, et al., 2025. A bandpass power combined amplifier based on all-ports reflectionless filtering power divider. *IEEE Trans Compon Packag Manuf Technol*, 15(4):792-799. https://doi.org/10.1109/TCPMT.2025.3545059